Journal of Alloys and Compounds 509 (2011) 8345–8349

Contents lists available at ScienceDirect

Journal of Alloys and Compounds

journal homepage: www.elsevier.com/locate/jallcom

Effect of α-Al_2O_3 on in situ synthesis low density O′-sialon multiphase ceramics

Yue Shao, Xiaolei Li*, Huiming Ji, Xiaohong Sun, Pei Cao

Key Laboratory for Advanced Ceramics and Machining Technology of Ministry of Education, School of Materials Science and Engineering, Tianjin University, Tianjin 300072, PR China

ARTICLE INFO

Article history:
Received 6 January 2011
Received in revised form 19 February 2011
Accepted 23 February 2011
Available online 4 March 2011

Keywords:
O′-sialon multiphase ceramics
α-Al_2O_3
Mechanism study
Phase composition
Lattice correction

ABSTRACT

In this paper, the effect of α-Al_2O_3 on in situ synthesis low density O′-sialon multiphase ceramics was investigated. Thermodynamics analysis was used to illustrate the feasibility of synthesizing O′-sialon at a low temperature of 1420 °C. The crystalline phase and microstructure were investigated by X-ray diffraction (XRD) and scanning electron microscope (SEM), respectively. The actual substitution parameter *x* value of O′-sialon was estimated via lattice correction. The results showed that, O′-sialon multiphase ceramics with different *x* values could be synthesized successfully through varying α-Al_2O_3 content. Bulk densities of samples ranging from 1.64 to 2.11 g cm^{-3} were adjusted with the percentage of α-Al_2O_3 increasing from 5.21 wt.% to 15.62 wt.%. Formation of nearly single-phase O′-sialon was obtained in the sample containing 10.42 wt.% α-Al_2O_3. The actual substitution parameter *x* increased with the increase of α-Al_2O_3, whereas it was lower than the original designation, and the O′-sialon with a low *x* value was achieved.

1. Introduction

Sialon ceramics were first proposed by Oyama and Kamigaito [1] and Jack and Wilson [2] in the early 70s and quickly developed as one of the attractive materials for high-temperature structural applications. According to the structure and components, there are α-sialon, β-sialon, O′-sialon and X-sialon in the sialon phases' family. Recently, sialon ceramics are attracting more and more attention due to its easy-sintering as well as retaining many excellent properties of silicon nitride, such as superior mechanical properties, thermal shock resistance and corrosion resistance [3–6]. Among all the single-phase sialon ceramics, O′-sialon ($Si_{2-x}A1_xO_{1+x}N_{2-x}$; $0 < x \leq 0.3$) has the best oxidation resistance due to a higher oxygen content than the other single-phase sialons [7]. Therefore, it is the most promising candidate in the development of elevated temperature thermal protective materials.

Previous studies have focused mainly on acquiring perfect mechanical properties, dielectric performance and thermal conductivity of Si_3N_4, β-sialon or their multiphase [8–13]. As for the research of O′-sialon, there were more involved with its multiphase fabricated with other additives, take TiO_2/(O′ + β′)-sialon, O′-sialon/SiC for example [14,15]. However, till now, the reports on the phase composition and lattice parameters analysis of O′-sialon are very scarce. It is well known that, phase composition and content are one of the most important parts among the factors that influence the performance of ceramics [16]. As a consequence, phase control process becomes the critical point for preparing O′-sialon ceramics with excellent properties. Besides, the O′-sialon multiphase ceramics reported in the literatures were usually prepared at very high sintering temperatures, which ranged from 1500 to 1950 °C [17–20].

In this work, in situ synthesis low density O′-sialon multiphase ceramics with different *x* values and content were fabricated by adjusting the α-Al_2O_3 amount at a low temperature of 1420 °C. The actual substitution parameter *x* value of O′-sialon was estimated via lattice correction. Furthermore, the relationship between α-Al_2O_3 amount and sintering behavior was also discussed.

2. Experimental procedures

2.1. Materials processing

O′-sialon was described as $Si_{2-x}A1_x\ O_{1+x}\ N_{2-x}$, with *x* varied from 0 to 0.30. Commercially available α-Si_3N_4 powder (the particle distribution $D50 < 2\ \mu m$), fused quartz powder ($D50 < 1\ \mu m$, chemical pure) and α-Al_2O_3 powder ($D50 < 1\ \mu m$, chemical pure) were employed as raw materials. Y_2O_3 (analytical pure) was used as the sintering aid. Just as the chemical reaction Eq. (3.1.3), different reactions with different stoichiometric ratios were achieved via varying *x* value, and the amount of raw materials including α-Al_2O_3 could be obtained. The external mass percentage of α-Al_2O_3 in relation to the total content of α-Si_3N_4 and fused quartz was 5.21 wt.%, 6.25 wt.%, 10.42 wt.% and 15.62 wt.%, corresponding to the *x* value 0.10, 0.12, 0.20 and 0.30, respectively. Different kinds of samples were fabricated and defined as B1, B2, B3 and B4. Fig. 1 indicates the positions of the starting compositions on the phase diagram of Si–Al–O–N system.

The starting powders were mixed by planetary milling in deionized water using zirconia balls for 4 h. The slurry was dried, granulated, and then passed through 40 mesh sieve. The green bodies were shaped into 36.80 mm × 6.36 mm × 5–6 mm by mold pressing and subsequently isostatically pressed under 100 MPa. After the

* Corresponding author. Tel.: +86 022 27890485.
E-mail address: lxlei@tju.edu.cn (X. Li).

0925-8388/$ – see front matter.
doi:10.1016/j.jallcom.2011.02.143

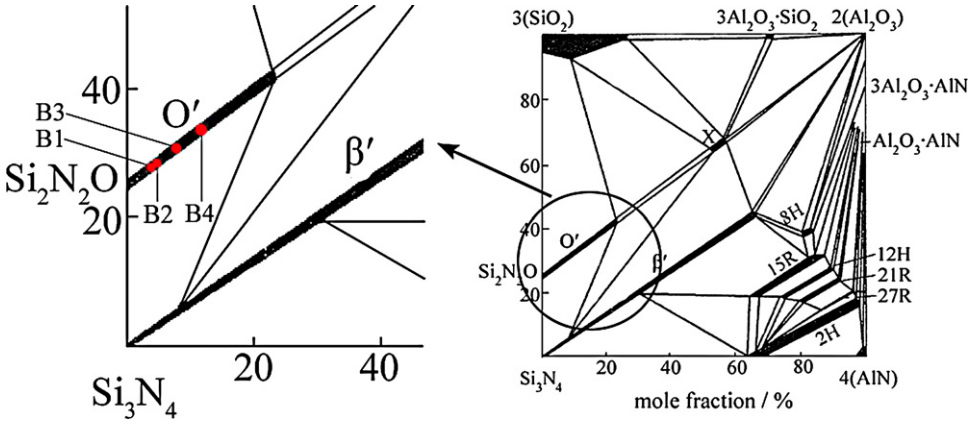

Fig. 1. Phase diagram of Si–Al–O–N system at 1750 °C [21].

volatilization of binder and water at 700 °C, the green bodies were sintered at 1420 °C in a furnace with a flowing nitrogen atmosphere.

2.2. Materials characterization

The bulk densities of the sintered products were measured by the Archimedes principle. Crystalline phases were identified by XRD (Rigaka D/max 2500 v/pc) using Cu Kα radiation as the radiation source, and the 2θ ranged from 10° to 60°. Because of orthorhombic system of O′-sialon, X-ray diffraction peaks of crystal plane were selected to determine the lattice parameters using the following equation:

$$d_{h\,k\,l} = \frac{1}{\sqrt{(h/a)^2 + (k/b)^2 + (l/c)^2}} \quad (2.2.1)$$

where $h\,k\,l$ was the crystal plane index; d_{hkl} was the distance between crystal planes of $(h\,k\,l)$; a, b and c were lattice parameters. The microstructure of the fracture surface of sintered samples after corrosion was characterized by scanning electron microscope (SEM, Hitachi/S-4800, Japan).

3. Results and discussion

3.1. Thermodynamics and phase analysis

A particular class of Si_3N_4 materials is of the O′-sialon, which is formed due to the solid solubility of Al_2O_3 and silicon oxynitride (Si_2N_2O) at a high sintering temperature, just as Eqs. (3.1.1) and (3.1.2) [21]:

$$\frac{1}{2}Si_3N_4 + \frac{1}{2}SiO_2 \rightarrow Si_2N_2O \quad (3.1.1)$$

$$\left(1 - \frac{x}{2}\right)Si_2N_2O + \frac{x}{2}Al_2O_3 \rightarrow Si_{2-x}Al_xO_{1+x}N_{2-x} \quad (3.1.2)$$

Based on Eqs. (3.1.1) and (3.1.2), the total chemical reaction Eq. (3.1.3) can be concluded:

$$\frac{1}{4}(2-x)Si_3N_4 + \frac{1}{4}(2-x)SiO_2 + \frac{x}{2}Al_2O_3 \rightarrow Si_{2-x}Al_xO_{1+x}N_{2-x} \quad (3.1.3)$$

Take $x = 0.20$ for example, the chemical reaction and corresponding molar Gibbs free energies of synthesizing O′-sialon ($Si_{1.8}Al_{0.2}O_{1.2}N_{1.8}$) phase are described as Eq. (3.1.4) and formula (3.1.5), respectively:

$$0.45Si_3N_4(s) + 0.45SiO_2(s) + 0.1Al_2O_3(s) \rightarrow Si_{1.8}Al_{0.2}O_{1.2}N_{1.8}(s) \quad (3.1.4)$$

$$\Delta_f G_T^\theta = \Delta_f G_{O'\text{-sialon}}^\theta - 0.45\,\Delta_f G_{Si_3N_4}^\theta - 0.45\,\Delta_f G_{SiO_2}^\theta - 0.1\,\Delta_f G_{Al_2O_3}^\theta \quad (3.1.5)$$

where $\Delta_f G_{O'\text{-sialon}}^\theta = -1024.8 + 0.291T$ kJ/mol; $\Delta_f G_{Si_3N_4}^\theta = -874.4 + 0.405T$ kJ/mol; $\Delta_f G_{SiO_2}^\theta = -956.4 + 0.198T$ kJ/mol; $\Delta_f G_{Al_2O_3}^\theta = -1682.9 + 0.323T$ kJ/mol [21]. And T is the absolute temperature.

Because the raw materials taking part in the reactions are condensed phase, the change of standard Gibbs free energies is $\Delta_f G_T^\theta = -37.15 - 0.01265T$ kJ/mol (Eq. (3.1.5)). When the sintering temperature (T) is 1693 K, $\Delta_f G_T^\theta = -58.57$ kJ/mol < 0, which illustrates that O′-sialon can be synthesized successfully by Si_3N_4, SiO_2 and Al_2O_3 at a low temperature of 1693 K. Meanwhile, according to the positions of starting compositions on the phase diagram (Fig. 1), $Si_{1.9}Al_{0.1}O_{1.1}N_{1.9}$, $Si_{1.88}Al_{0.12}O_{1.12}N_{1.88}$, $Si_{1.8}Al_{0.2}O_{1.2}N_{1.8}$ and $Si_{1.7}Al_{0.3}O_{1.3}N_{1.7}$ can be obtained in theory after complete reaction.

Fig. 2 shows the XRD patterns of the aforementioned samples. The samples mainly consisted of O′-sialon phase. In addition, a spot of β-Si_3N_4 was detected, indicating the incomplete reaction of Si_3N_4. Moreover, no α-Si_3N_4 phase was detected in the diffraction patterns (Fig. 2), confirming a full transformation from α-Si_3N_4 to β-Si_3N_4 during current sintering temperature.

The quantitative phase analysis was finished by matrix-flushing method [22] and listed in Table 1. The O′-sialon content became larger as the amount of α-Al_2O_3 increased. During densification, because the formation of O′-sialon depended on the liquid phase [23,24], the larger amount of O′-sialon phase was mostly attributed to the higher amount of α-Al_2O_3 which could generate more vol-

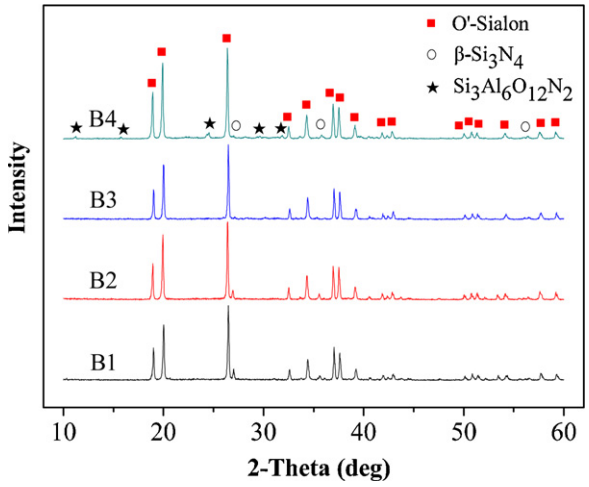

Fig. 2. XRD patterns of the samples with different α-Al_2O_3 contents sintered at 1420 °C.

Table 1
XRD quantitative analysis results of the samples.

Samples	O′-sialon (wt.%)	β-Si_3N_4 (wt.%)	$Si_3Al_6O_{12}N_2$ (wt.%)
B1	95.09	4.91	0
B2	95.96	4.04	0
B3	98.88	1.12	0
B4	96.52	1.44	2.04

Table 2
Cell parameters and unit cell volumes of O′-sialon in the samples.

Samples	*a* (nm)	*b* (nm)	*c* (nm)	*v* (nm^3)
B1	0.887525	0.549147	0.484842	0.23630
B2	0.887632	0.549163	0.484932	0.23638
B3	0.888337	0.549208	0.485138	0.23669
B4	0.889062	0.549512	0.485362	0.23712

ume of liquid phase with other additives to increase the mass transfer rate and promote nucleation. Formation of nearly single-phase O′-sialon was obtained in the sample containing 10.42 wt.% α-Al_2O_3. According to the XRD patterns in Fig. 2, when the designed *x* value was 0.30, $Si_3Al_6O_{12}N_2$ phase was observed, probably due to the reaction between Si_3N_4 and α-Al_2O_3. However, the reaction was not occurred in other samples result from the insufficient α-Al_2O_3 content. As a result, the amount of O′-sialon in B4 decreased although it had the most amount of α-Al_2O_3. Duan et al. [19] hold that during cooling, a part of the liquid phase formed at the sintering temperature crystallized to form an intergranular crystalline phase, and the residual liquid phase formed the intergranular glass phase. As shown in Fig. 2, the XRD patterns of samples were not smooth enough and no raw materials were detected, suggesting that some of raw materials reacted and formed intergranular glass phase which was amorphous.

3.2. Actual substitution parameter x with different α-Al_2O_3 amounts

The analysis of XRD patterns showed that O′-sialon phase and some unreacted β-Si_3N_4 were found in the samples. In order to identify the actual substitution parameter *x* of O′-sialon in this research, the cell parameters and unit cell volumes of the O′-sialon phase in the ceramics were refined by a software jade 5.0, calculated by Eq. (2.2.1) and listed in Table 2. The published data of O′-sialon phase with different *x* values were collected in Table 3 [19]. Cell parameter *a* change with substitution parameter *x* of O′-sialon was drawn in Fig. 3 and exhibited a good nonlinear fitting of calculation. The formula after curve fitting could be represented by Eq. (3.2.1):

$$y = 0.89363 - 0.0065 \times \exp\left(-\frac{x}{0.29087}\right) \quad (3.2.1)$$

In comparing the cell parameter values *a* of O′-sialon in Table 2 with those in the curve of Fig. 3 or Eq. (3.2.1), it could be concluded that the actual *x* values of O′-sialon were 0.018 in B1, 0.023 in B2, 0.060 in B3, and 0.103 in B4, respectively.

On the basis of the data from Table 2, increased in the unit cell dimensions of the O′-sialon with increasing *x* value was anticipated as a result of the replacement of Si–N bonds (~0.174 nm) by A1–O (~0.175 nm). The actual substitution parameter *x* calculated through Eq. (3.2.1) raised with increasing α-Al_2O_3 content. However, it was lower than the original designation, which meant

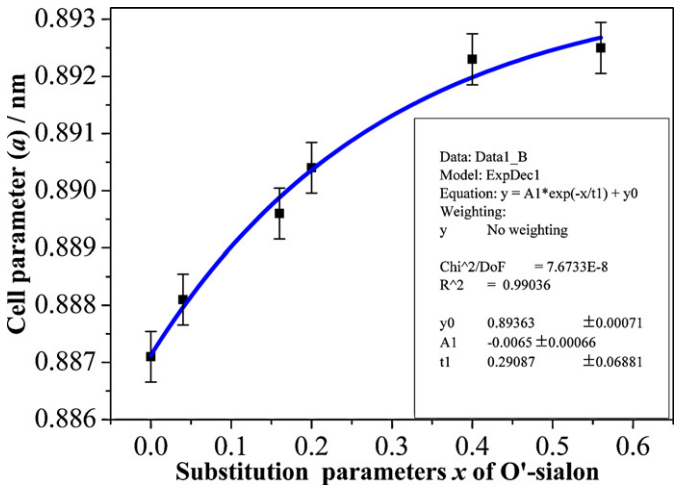

Fig. 3. Cell parameter *a* changes with substitution parameter *x* of O′-sialon.

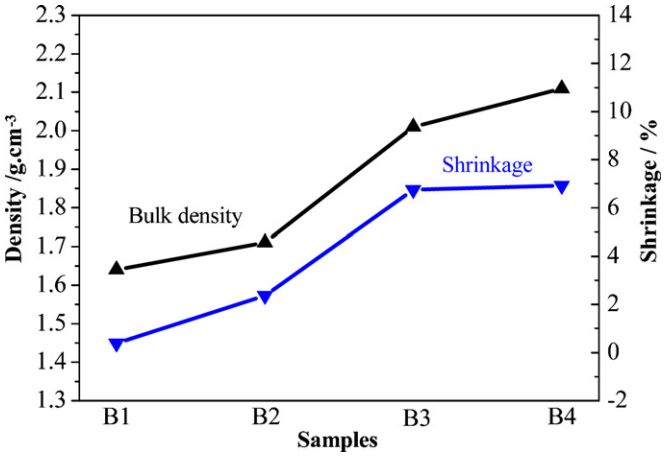

Fig. 4. The densities and shrinkage of samples sintered at 1420 °C.

only a spot of α-Al_2O_3 diffuse into Si_2N_2O crystal lattice, and the O′-sialon with a low *x* value was achieved. Al_2O_3 is very active as a sintering additive of Si_3N_4 ceramics [25] and the formation of Si_2N_2O crystals must proceed in a liquid phase [26], so the result also implied that α-Al_2O_3 was firstly used as sintering aid to form liquid phase with other additives which could promote the transformation from α-Si_3N_4 to β-Si_3N_4 and the formation of Si_2N_2O. This process decreased the actual substitution content of α-Al_2O_3. Subsequently, the O′-sialon phase would be achieved through the reaction of residual α-Al_2O_3 and Si_2N_2O (Eq. (3.1.2)). Furthermore, the formation of $Si_3Al_6O_{12}N_2$ phase (Fig. 2-B4) was occurred simultaneously with solid solution reaction, and the actual *x* value in B4 could not increase continually with increase the content of α-Al_2O_3.

3.3. Relationship between α-Al_2O_3 amount and sintering behavior

The densities and shrinkage of samples sintered at 1420 °C were plotted in Fig. 4. It could be seen that, B1 had the lowest den-

Table 3
Cell parameters of O′-sialon from published data (JCPDS cards).

x of O′-sialon	0	0.04	0.16	0.17	0.20	0.40	0.56
a (nm)	0.8871	0.8881	0.8896	0.8893	0.8904	0.8923	0.8925
JCPDS#	79-1539	42-1492	42-1491	88-2058	40-0672	42-1490	88-2060

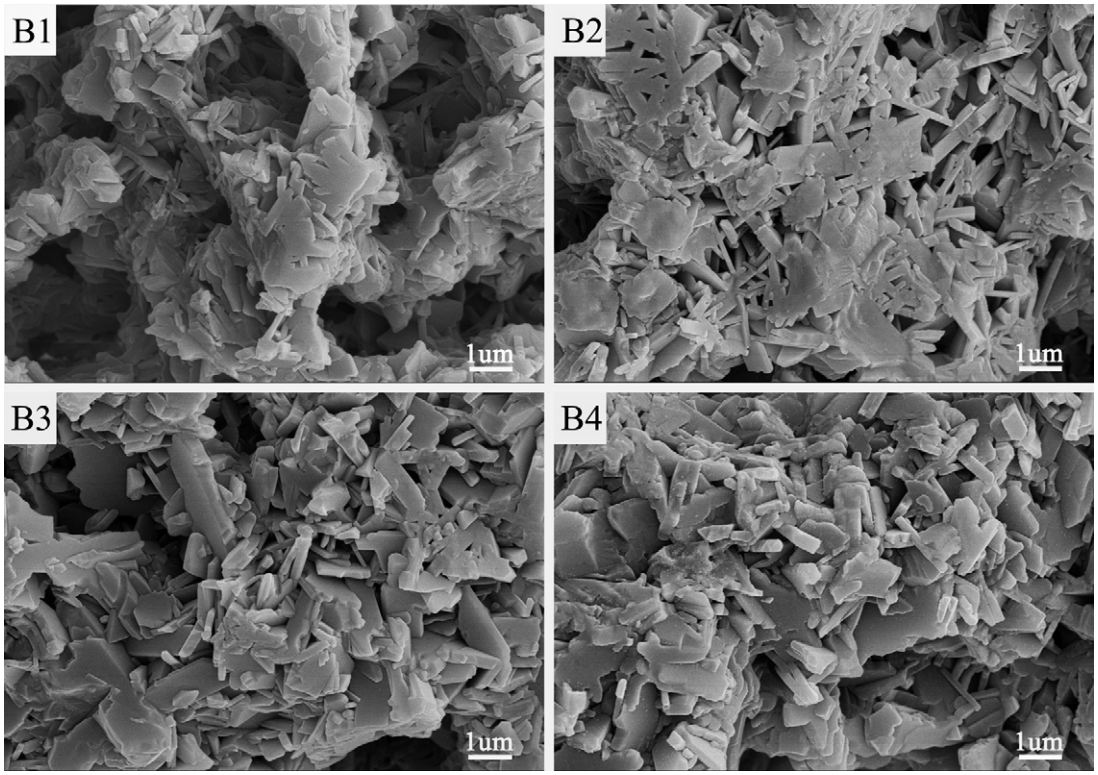

Fig. 5. The microstructure of the fracture surface of the samples with varying α-Al_2O_3 content sintered at 1420 °C.

sity (1.64 g cm^{-3}) and the shrinkage was 0.39%. When the mass percentage of α-Al_2O_3 increased from 5.21 wt.% to 15.62 wt.%, the shrinkage varied from 0.39% to 6.92%, and the range of bulk density was 1.64–2.11 g cm^{-3}.

Fig. 5 shows the microstructure of the fracture surface of samples with varying α-Al_2O_3 content sintered at 1420 °C. Regardless of different α-Al_2O_3 contents, all samples mainly consisted of slat-like O′-sialon grains, as also evidenced by XRD results (Fig. 2). It could be seen that some big pores existed both in samples B1 and B2, formed by the burning of binder and water as well as the bridging and overlapping of the grains. Samples B3 and B4 became more dense with α-Al_2O_3 increasing, corresponding to the results in Fig. 4.

As stated above, liquid phase could preferentially dissolve the solid phase and promote dissolution-precipitation process. This process was accompanied by the precipitation of O′-sialon nuclei. On one hand, Trigg and Jack [24] consider that the densification rate increases with aluminium concentration and hence increasing volume of liquid. The more amount of liquid phase formed in B3 and B4 could bind the grains together, fill the pores and lead to a greater densification. On the other hand, the thin slat-like O′-sialon grains could be observed in samples B1 and B2 from Fig. 5, but thick slat-like grains were found in B3 and B4. Owing to the increase of α-Al_2O_3 amount, the O′-sialon grains growth also promoted the densification. Consequently, the samples with different bulk densities could be prepared with different α-Al_2O_3 amounts.

4. Conclusions

In situ formed low density O′-sialon multiphase ceramics with different *x* values and content were fabricated successfully via adjusting α-Al_2O_3 amount at a low temperature of 1420 °C. The effect of α-Al_2O_3 could be concluded as follows: (1) α-Al_2O_3 was used as sintering aid to form liquid phase with other additives, which could promote the transformation from α-Si_3N_4 to β-Si_3N_4 and the formation of Si_2N_2O. (2) The slat-like O′-sialon phase would be achieved through the reaction of residual α-Al_2O_3 and Si_2N_2O. (3) The reaction maybe also occurred by α-Al_2O_3 and Si_3N_4 to form crystalline phases. The actual substitution parameter *x* raised as the amount of α-Al_2O_3 increased, whereas it was lower than the original designation, and the O′-sialon with a low *x* value was achieved. Formation of nearly single-phase O′-sialon was obtained in the sample containing 10.42 wt.% α-Al_2O_3. Bulk densities of samples ranging from 1.64–2.11 g cm^{-3} were adjusted with the percentage of α-Al_2O_3 increasing from 5.21 wt.% to 15.62 wt.%, owing to the presence of higher volume liquid with increase aluminium concentration.

Acknowledgement

The work was supported by the Natural Science Foundation of China (Grant No. 50872090).

References

[1] Y. Oyama, O. Kamigaito, J. Appl. Phys. 10 (11) (1971) 1637.
[2] K.H. Jack, W.I. Wilson, Nat. Phys. Sci. 238 (80) (1972) 28.
[3] Y. Inagaki, N. Kondo, T. Ohji, J. Eur. Ceram. Soc. 22 (2002) 2489–2494.
[4] J.H. She, J.F. Yang, D.J. Daniel, N. Kondo, T. Ohji, S. Kanzaki, Y. Inagaki, J. Am. Ceram. Soc. 86 (4) (2003) 738–740.
[5] Y. Zhang, Y.B. Cheng, S. Lathabai, K. Hirao, J. Am. Ceram. Soc. 88 (1) (2005) 114–120.
[6] H.J. Wang, J.L. Yu, J. Zhang, D.H. Zhang, J. Mater. Sci. 45 (2010) 3671–3676.
[7] X.M. Hou, K.C. Chou, J. Univ. Sci. Technol. Beijing 29 (2007) 1114 (in Chinese).
[8] C.H. Lee, H.H. Lu, C.A. Wang, P.K. Nayak, J.L. Huang, J. Alloys Compd. 508 (2010) 540–545.
[9] X.M. Li, L.T. Zhang, X.W. Yin, Z.J. Yu, J. Alloys Compd. 490 (2010) 40–43.
[10] H.L. Du, Y. Li, C.B. Cao, J. Alloys Compd. 503 (2010) 9–13.
[11] G.H. Peng, M. Liang, Z.H. Liang, J. Am. Ceram. Soc. 92 (9) (2009) 2122–2124.
[12] O. Eser, S. Kurama, G. Gunkaya, J. Eur. Ceram. Soc. 30 (2010) 2985–2990.
[13] Y.F. Xia, Y.P. Zeng, D.L. Jiang, Ceram. Int. 35 (2009) 1699–1703.
[14] H.S. Hao, L.H. Xu, M. Liu, X.M. Zhang, J.Y. Yang, Y.J. Guo, Mater. Sci. Forum 610–613 (2009) 267.
[15] J. Yang, L.M. Pen, X.X. Xue, M. Wang, T. Qiu, J. Rare Earth 27 (2) (2009) 204.
[16] P.F Becher, G.S. Painter, N. Shibata, R.L. Satet, M.J. Hoffmann, S.J. Pennycook, Mater. Sci. Eng. A 422 (2006) 85–91.

[17] M. Ohashi, K. Hirao, M.E. Briton, N. Takaaki, M. Yasuoka, S. Kanzaki, J. Am. Ceram. Soc. 76 (8) (1993) 2112–2114.
[18] B.T. Lee, H.G. Jeong, K. Hiraga, Mater. Trans. 43 (1) (2002) 19–23.
[19] R.G. Duan, G. Roebben, J. Vleugels, O. Van der Biest, Mater. Sci. Eng. A 427 (2006) 195–202.
[20] T. Jiang, X.X. Xue, P.N. Duan, G. Du, Acta Metall. Sin. 43 (2) (2007) 131–136 (in Chinese).
[21] Z.Y. Chen, Chemical Thermodynamics of Refractories, Metallurgical Industry Press, Beijing, 2005.
[22] F.H. Chung, J. Appl. Cryst. 7 (1974) 519–525.
[23] X.W. Xu, H. Liang, X.L. Li, H.M. Ji, H.X. Lu, Y.Z. Wan, Rare Metals 29 (2) (2010) 214.
[24] M.B. Trigg, K.H. Jack, J. Mater. Sci. 23 (1988) 481–487.
[25] J.F. Yang, Y. Beppu, G.J. Zhang, T. Ohji, S. Kanzaki, J. Am. Ceram. Soc. 85 (7) (2002) 1879–1881.
[26] R.G. Duan, G. Roebben, J. Vleugels, O. Van der Biest, Acta Mater. 53 (2005) 2547–2554.